Theoretical and Experimental Study of Wind- and Wave-Induced Drift

D. T. TSAHALIS

Shell Development Company, Westhollow Research Center, Houston, TX 77001

(Manuscript received 21 July 1978, in final form 13 August 1979)

ABSTRACT

A study has been carried out of the surface drift on open water due to the combined action of currents, winds and wind-generated waves for cocurrent and countercurrent air flow. It has been shown theoretically that the nondimensional groups necessary for the modeling of the surface drift are $(T - c)/c$ and U_{10}/c, where U_{10}, T and c are the wind, water surface and current velocities, respectively, the wind being measured at the uniquely adopted height of 10 m. Surface drift experiments, carried out in a current tank/wind tunnel, have verified the dependence on the above groups and led to the derivation of relationships for the calculation of the total surface drift. The surface drifts, calculated from the above relationships, are in excellent agreement with available field and laboratory data. The present results support Charnock's expression relating the surface roughness and shear velocity for completely rough flow due to gravity waves and Wu's Froude number scaling of wind-stress coefficients. Furthermore, the present results show that wind-generated waves generally cause a net decrease or increase of the surface drift for cocurrent and countercurrent air flow, respectively. Finally, laws have been formulated for the scaling of current tank/wind tunnel data for wind velocities and significant wave heights to prototype (atmospheric boundary layer) conditions.

1. Introduction

Accidental oil spills occur regardless of the measures taken to prevent their occurrence. In order to assess the environmental risk and properly deploy clean-up resources, it is necessary that the motion (drift) of oil spills under the influence of currents, winds and wind-generated waves can be predicted.

It is generally accepted, without formal proof, that the drift of oil on the water surface is the same as the surface drift of uncontaminated water, provided that the thickness of the oil film is small. Surface drift of water is generated by the combined action of currents, either tidal or residual, and winds. Winds generate both surface drift (wind-induced drift) through wind shear action and waves. Waves, in turn, contribute to the surface drift (wave-induced drift) through Stokes mass transport. A number of researchers have investigated theoretically and experimentally in the field and the laboratory the separate or combined effect of currents, winds and waves on the surface drift.

Theoretically, Kraus (1977) showed that for turbulent flow the surface drift with currents present is the vector mean of the current velocity and the surface geostrophic wind weighted by the square root of the ratio of the air density to the water density. For zero current velocity, he predicted that the surface drift is ~3.4% of the surface geostrophic wind. However, Kraus did not include in his analysis the effect of wind-generated waves on the surface drift. Madsen (1977) introduced a physically realistic and general model for the vertical eddy viscosity in a homogeneous fluid and showed that the surface drift in the absence of currents is ~3% of the wind velocity measured at a height of 10 m.

In the laboratory, Keulegan (1951) found the surface drift to be ~3.3% of the mean wind velocity through his wind tunnel and independent of surface waves. Fitzgerald (1964) found the surface drift, over wavy water, to be ~3% of the wind velocity measured at 2 cm height above the mean water surface. Wu (1968) found the surface drift to increase with the wind speed and become asymptotically 4.8% of the free-stream wind speed as the waves start to break. Schwartzberg (1970) found the surface drift to be ~3.1% of the mean wind velocity through his wind tunnel. By extrapolating his results to infinite height of the wind tunnel, he predicted that on open water the surface drift should be 3.7% of the wind velocity. Plate and Trawle (1970), and Wright and Keller (1971) found the surface drift to be 2.6 and 4.45% of the free-stream wind speed, respectively. The studies of Schwartzberg and Plate *et al.* merit special attention because they are the only investigations where the combined effect of current and wind on the surface drift has been considered. They demonstrated that the total surface drift cannot be determined by

0022-3670/79/061243-15$07.75

TABLE 1. Wind-induced drifts determined by different investigators for zero current.

Author	Method of determination	Surface drift*
Laboratory experiments		
Keulegan (1951)	Small paraffin particles	0.033 $\bar{U}$
Fitzgerald (1964)	Particles of talc	0.03 $U_{0.02}$
Wu (1968)	Spherical floats	0.048 U_a
Schwartzberg (1970)	Paraffin oil lenses	0.031 $\bar{U}$
Plate & Trawle (1970)	Paper discs (wax-covered)	0.026 U_a
Wright & Keller (1971)	Paraffin & polyethylene floats	0.045 U_a
Shemdin (1972)	Water soaked paper discs	0.03 U_a
Field experiments		
Van Dorn (1953)	Cork floats	0.033 U_{10}
Hughes (1956)	Plastic envelopes	0.033 U_{10}
Tomczak (1964)	Post cards	0.042 U_{10}
J. E. Smith (1968)	Torrey Canyon oil spill	0.033 U_{10}
C. L. Smith (1974)	Oil No. 2, 4, 6	0.036 U_{10}

* $\bar{U}$, mean wind velocity in the wind tunnel; U_a, free-stream velocity in the wind tunnel; $U_{0.02}$, U_{10}, wind velocity measured at 0.02 and 10 m above the mean water surface, respectively.

the simple superposition of the current and wind-induced drifts. Finally, Shemdin (1972) found the surface drift to be ~3% of the free-stream velocity.

In the field, Van Dorn (1953) performed experiments in a basin and found the surface drift to be 3.3% of the wind speed at 10 m height and independent of waves. Hughes (1956) measured the drift of floating plastic envelopes in the Atlantic Ocean and found the surface drift to be ~3.3% of the wind speed at 10 m height. Tomczak (1964) studied the drift of post cards as well as the track of the oil spill from the *Gerd Maersk* (1955) in the shallow waters off Germany and Denmark and determined the surface drift to be 4.2% of the wind speed at 10 m height. However, it is suspected that tidal and coastal currents have influenced Tomczak's estimate of surface drift. J. E. Smith (1968) was able to predict reasonably well the movement of the oil spill from the *Torry Canyon* (1967) by utilizing a surface drift of 3.3% of the wind speed at 10 m height. Finally, C. L. Smith (1974) studied experimental oil spills in the Chesapeake Bay and found the surface drift to be ~3.6% of the wind speed at 10 m height.

The results on surface drift, reported in the above cited references, are summarized in Table 1. From the surface drifts determined in the field, it is concluded that the combined wind- and wind-generated wave-induced drift, in the absence of currents and a fully developed sea, is ~3.3% of the wind velocity at 10 m height.

Waves not only contribute to the surface drift through Stokes mass transport but also affect the wind-induced drift through the wind shear which depends on the roughness of the water surface. Alofs and Reisbig (1972) studied in a water tank the wave-induced drift of oil lenses which were subjected to mechanically generated gravity waves. They measured surface drifts which were higher by 35–150% than those predicted by the Stokes theory of deep water waves. Later, Reisbig *et al.* (1973) studied experimentally the surface drift of oil lenses which were subjected to the separated and coupled effects of wind and mechanically generated waves. Both the wind and the waves traveled in the same direction. Their results clearly demonstrate that the wind-induced drift and the wave-induced drift cannot be simply superimposed to yield the combined surface drift. Furthermore, they found that the air turbulence intensity has no effect on the surface drift. Schwartzberg (1970), using average wave heights taken from the wind-wave spectra of Pierson *et al.* (1955), calculated the wave-induced drift to be less than 0.65% of the wind speed for wind speeds up to 50 kt. Bye (1967) and Kenyon (1969) suggested that the wind-induced drift in a fully developed sea is primarily due to Stokes transport. Shemdin (1972), using the relationship for the wind-induced drift proposed by Bye, calculated surface drifts which were one order of magnitude smaller than the experimentally measured values.

The major conclusion, drawn from the findings of the above cited references, is that the surface drift due to the combined action of currents, winds and waves cannot be determined by the simple superposition of the separately determined current, wind- and wave-induced drifts. Also, considering the present poor understanding of the mechanism by which momentum and kinetic energy is transmitted and divided between waves and drift currents (see Monin, 1969), it is evident that in an experimental investigation of the surface drift, currents, winds and waves must be considered simultaneously.

In this paper, the results of a theoretical and experimental study of the surface drift due to the combined effect of currents, winds and wind-generated waves are presented for cocurrent and countercurrent air flows.

2. Analytical considerations

Let c be the uniform current velocity and U_h the free-stream wind velocity measured at height h, i.e., the edge of the atmospheric boundary layer. The direction of c is taken to be positive and U_h is positive or negative for cocurrent or countercurrent air flow, respectively. Let T be the surface drift velocity due to the combined action of current, wind and wind-generated waves. T is also positive or negative if the water surface is traveling in the same or opposite direction with the current c, respectively.

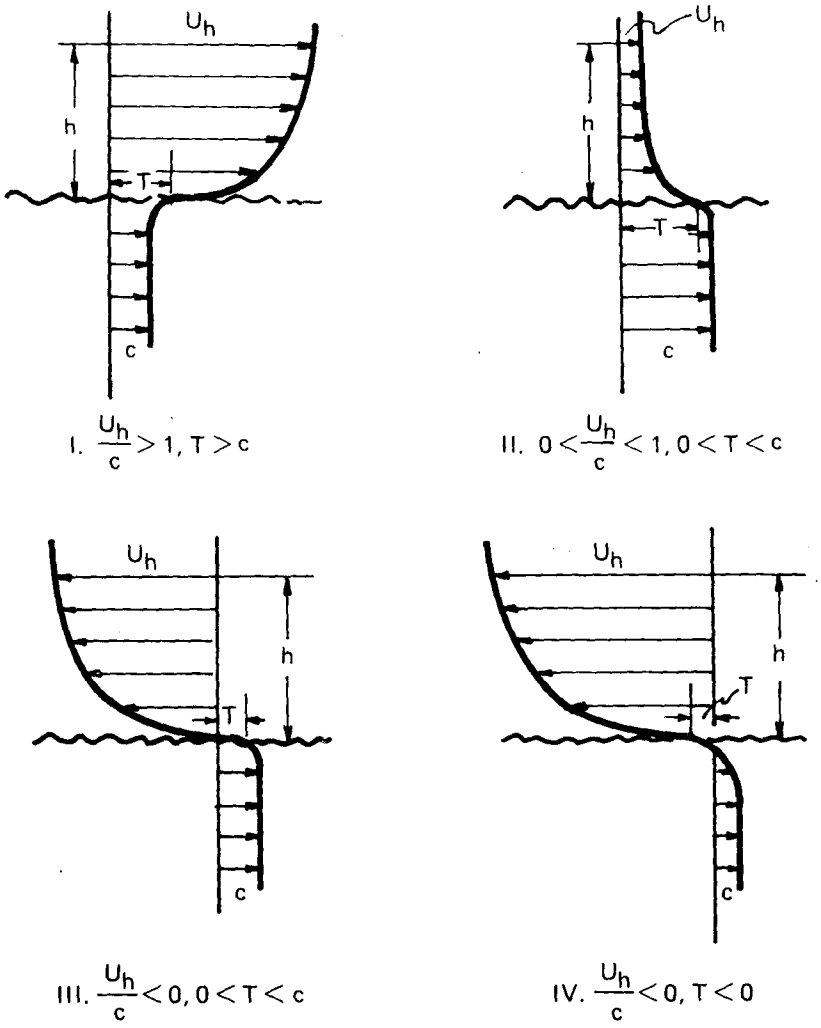

FIG. 1. Schematics of different flow configurations for cocurrent and countercurrent air flow.

For a given current velocity c, four distinct flow configurations are easily identified (see Fig. 1) depending on the magnitude and direction of U_h. For an observer moving with the water surface, the water at a large depth is moving with velocity $c - T$ and the air at height h is moving with velocity $U_h - T$. At the air-water interface, the shear stress exerted by the air, moving with velocity $U_h - T$, minus the wave stress, i.e., the rate of direct momentum transfer from the wind to waves, is equal to the shear stress exerted by the water, moving with velocity $c - T$. Wu (1975) has shown that the wave stress is generally ~36% of the wind stress, except at very low wind velocities. Therefore,

$$C_w \rho_w (c - T)^2/2 = 0.64 C_a \rho_a (U_h - T)^2/2, \quad (1)$$

where C_w and C_a are the friction factors and ρ_w and ρ_a are the densities of the water and the air, respectively. Assuming that the flow in both the water and the air is turbulent and that the wavy air-water interface can be replaced by a rough flat plate, the friction factors can be calculated approximately from the relationships

$$\left.\begin{aligned} C_w &= K\left(\frac{L|c - T|}{\nu_w}\right)^n \\ C_a &= K\left(\frac{L|U_h - T|}{\nu_a}\right)^n \end{aligned}\right\}, \quad (2)$$

where ν_w and ν_a are the kinematic viscosities of the water and the air, respectively, L is the fetch and K and n are characteristic constants. For large Reynolds number and constant fetch, the exponent n can be taken equal to $-1/5$ (see Schlichting, 1968). Substituting Eq. (2) into (1), gives

$$\left(\frac{|c - T|}{|U_h - T|}\right)^n \left(\frac{c - T}{U_h - T}\right)^2 = 0.64 \frac{\rho_a}{\rho_w}\left(\frac{\nu_w}{\nu_a}\right)^n. \quad (3)$$

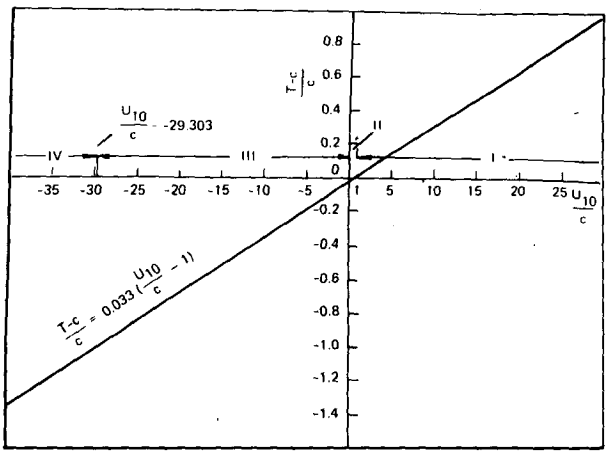

FIG. 2. The function $(T - c)/c = f(U_{10} - c)$ for the surface drift velocity from Eq. (8).

It is deduced from Fig. 1 that for

Case I:

$$\frac{|c - T|}{|U_h - T|} = \frac{T - c}{U_h - T},$$

because

$$c - T < 0, \quad U_h - T > 0. \tag{4}$$

Cases II–IV:

$$\frac{|c - T|}{|U_h - T|} = \frac{T - c}{U_h - T},$$

because

$$c - T > 0, \quad U_h - T < 0. \tag{5}$$

Substituting Eqs. (4) and (5) into (3), yields

$$\frac{T - c}{c} = \left[1 + \left(\frac{\rho_w}{0.64\,\rho_a}\right)^{1/(n+2)} \times \left(\frac{\nu_a}{\nu_w}\right)^{n/(n+2)}\right]^{-1} \left(\frac{U_h}{c} - 1\right). \tag{6}$$

Eq. (6) holds for all four flow-configurations shown in Fig. 1. Substituting $n = -1/5$ and values for the densities and the kinematic viscosities of the air and the water at 68°F gives

$$\frac{T - c}{c} = 0.0245\left(\frac{U_h}{c} - 1\right). \tag{7}$$

For $c = 0$, Eq. (7) yields $T = 0.0245U_h$ or $T = 2.45\%$ of U_h. As pointed out earlier, however, U_h is the free-stream wind velocity measured at height h, i.e., the edge of the atmospheric boundary layer. Therefore, if U_h is replaced by the wind velocity at a height of 10 m, U_{10}, then the constant in Eq. (7) should be increased accordingly in order to take into account the fact that $U_{10} < U_h$. Considering, however, that the surface drift for zero current and fully developed sea is 3.3% of U_{10}, it is argued that the adjusted value of the constant is 0.033, i.e.,

$$\frac{T - c}{c} = 0.033\left(\frac{U_{10}}{c} - 1\right). \tag{8}$$

Eq. (8) has been plotted in Fig. 2 where the regimes corresponding to the different flow configurations of Fig. 1 are also shown.

Besides the established surface drift of 3.3% of U_{10} in the absence of current and fully developed sea, the surface drift can be predicted for special cases on physical arguments. Specifically, for $U_{10} = c$ the surface drift is equal to U_{10} and c due to the absence of wind shear, i.e., $T = U_{10} = c$. For $U_{10} = 0$ and $c \neq 0$ the surface drift is slightly smaller than c due to the retarding action of the stagnant air, that is, $T = c - \epsilon$, where $\epsilon \ll c$. For c = constant and $|(U_{10}/c)| > |(U_{10}/c)_{cr}|$, where $|(U_{10}/c)_{cr}|$ is some large number, the combined wind- and wind-generated wave-induced drift can be calculated as if the wind was blowing over stagnant water, $T \approx c + 0.033\,U_{10}$. It is very interesting to note that in spite of its simplicity, Eq. (8) predicts surface drifts for these special cases which are in agreement with the above quantitative and qualitative arguments. These predictions are summarized in Table 2. Furthermore, Eq. (8) indicates that the nondimensional groups necessary for the modeling of surface drift, at least over the range of applicability of (8), are

$$\frac{T - c}{c} \quad \text{and} \quad \frac{U_{10}}{c}, \tag{9}$$

and that c is the appropriate representative velocity to be used for the nondimensionalization of velocities.

The effect of the wave-induced drift on the combined current and wind-induced drift given by Eq. (8) has not been taken into account yet. Having in mind the arguments of the previous paragraph, this effect is confined in the range of wind and current velocities satisfying the relationship $|(U_{10}/c)| < |(U_{10}/c)_{cr}|$, where $|(U_{10}/c)_{cr}|$ might not be the same for $U_{10}/c > 0$ and $U_{10}/c < 0$. Considering that for

TABLE 2. The surface drift velocity T for special flow configurations.

Flow configuration	Surface drift velocity: Predicted on physical arguments	Surface drift velocity: Calculated from Eq. (8)
$U_{10} = c$	$T = U_{10} = c$	$T = U_{10} = c$
$U_{10} = 0, \quad c \neq 0$	$T = c - \epsilon, \quad \epsilon \ll c$	$T = 0.967c$
$\left\|\frac{U_{10}}{c}\right\| > \left\|\left(\frac{U_{10}}{c}\right)_{cr}\right\|$	$T \approx c + 0.033U_{10}$	$T \approx c + 0.033U_{10}$
$U_{10} \neq 0, \quad c = 0$	$T = 0.033U_{10}$*	$T = 0.033U_{10}$

* Field experiments.

constant air and water physical properties, constant fetch and no swell, the state of locally saturated waves that determines the contribution of the wave transport depends only on c and U_{10}, it is argued that the total surface drift can be modeled in terms of the nondimensional groups of (9). That is, for

$$\left|\frac{U_{10}}{c}\right| < \left|\left(\frac{U_{10}}{c}\right)_{cr}\right|,$$

$$\frac{T-c}{c} = f(\text{current, wind, wave}) = f\left(\frac{U_{10}}{c}\right), \quad (10)$$

where

$$\left.\begin{aligned} \lim f\left(\frac{U_{10}}{c}\right) &\to 0 \\ \left|\frac{U_{10}}{c}\right| &\to 1 \end{aligned}\right\}, \quad (11)$$

$$\left.\begin{aligned} \lim f\left(\frac{U_{10}}{c}\right) &\to 0.033\left(\frac{U_{10}}{c} - 1\right) \\ \left|\frac{U_{10}}{c}\right| &\to \left|\left(\frac{U_{10}}{c}\right)_{cr}\right| \end{aligned}\right\}. \quad (12)$$

For $|(U_{10}/c)| > |(U_{10}/c)_{cr}|$, Eq. (10) is replaced by Eq. (8). The experiments described later in the paper were undertaken in order to (a) determine the function $f(U_{10}/c)$ and (b) verify the assumption that for $|(U_{10}/c)| > |(U_{10}/c)_{cr}|$, where $(U_{10}/c)_{cr}$ remains to be determined, the total surface drift is given by Eq. (8).

3. Scaling laws

The major problem encountered in any laboratory study of wind-induced drift is the scaling of model (laboratory) results, for wind velocities measured at a certain height from the mean water surface, to prototype (atmospheric boundary layer) conditions of wind velocities at the uniquely adopted height of 10 m. This basic fact has been ignored by some investigators in this field and is responsible for disparities that exist between model and prototype results. The problem of scaling laws was addressed in the present investigation and a method was developed for scaling up model results to prototype. This method is discussed below.

It has been established experimentally (see Ruggles, 1969; Plate, 1971) that the wind velocity profile is logarithmic in at least the lowest 50–60 ft of the atmospheric boundary layer, down to the lowest distances from the ground or water surface. This is the only portion of the atmospheric boundary layer that can be modeled exactly in the laboratory. Its counterpart is the logarithmic portion of the boundary layer over a flat plate. It has also been established experimentally by Wu (1968) and Shemdin (1972), and verified in the present investigation, that in wind-tunnel experiments of wind-induced drift the wind velocity profile is logarithmic near the water surface.

Modeling of the logarithmic portion of the atmospheric boundary layer over a fixed surface means exact scaling of the logarithmic law. Scaling requires (see Plate, 1971) that the shear velocity u_* and the ratio h/k be the same in the model and the prototype, where k is the surface roughness and h a scaling length such as the dimension of a terrain feature. Since in the present problem the water surface is moving, it is also required that the surface velocity T be the same in the model and the prototype. This condition is satisfied if the current c is also the same in the model and the prototype. The above conclusion is easily reached if one considers that 1) the wind-induced drift follows a logarithmic distribution when plotted downward with respect to the surface (Bye, 1967); Shemdin, 1972); 2) the water shear stress is ~64% of the air shear stress except at very low wind velocities (Wu, 1975); and 3) the air shear velocity and the ratio h/k are the same in the model and the prototype, where h in the present problem is the significant wave height $H_{1/3}$ (the average wave height of the largest one-third of recorded waves). Summarizing, exact scaling of the logarithmic portion of the atmospheric boundary layer in the present problem requires that the air shear velocity u_*, the ratio of significant wave height to surface roughness $H_{1/3}/k$ and the current velocity c be the same in the model and the prototype. A direct consequence of the above conditions is that the surface drift is also the same in the model and the prototype. Furthermore, in order to assure independence of the flow from the Reynolds number, it is also required that $u_*k/\nu_a > 70$. Coriolis forces are negligible compared to viscous forces in the logarithmic portion of the atmospheric boundary layer and they are not considered in the modeling.

The velocity distributions in the logarithmic portion of the turbulent boundary layer in the model and the prototype, for flow over a completely rough surface ($u_*k/\nu_a > 70$), are given by Schlichting (1968) as

$$\frac{u_m - T_m}{u_{*m}} = 5.75 \log\left(\frac{y_m}{k_m}\right) + 8.5, \quad (13)$$

$$\frac{U_{10} - T_p}{u_{*p}} = 5.75 \log\left(\frac{y_p}{k_p}\right) + 8.5, \quad (14)$$

where k_m and k_p are the surface roughnesses, y_m and $y_p = 10$ m ≈ 32.8 ft are the heights at which the wind velocities are measured, T_m and T_p are the surface drifts, u_m and U_{10} are the wind velocities, and u_{*m} and u_{*p} are the shear velocities of the model and the prototype, respectively. It is im-

portant to mention at this point that Wu (1968) established experimentally that the constant of proportionality in Eqs. (13) and (14) is, indeed, the universal constant (5.75) in the Kármán-Prandtl velocity distribution. Subtracting Eq. (13) from Eq. (14) and taking into account the conditions for exact scaling, yields

$$U_{10} = u_m - u*5.75 \log \left(\frac{y_m}{y_p} \frac{k_p}{k_m} \right). \quad (15)$$

If the ratio k_p/k_m is known, Eq. (15) is the scaling law for velocities between the model and the prototype. Note that the ratio k_p/k_m is independent of the current velocity c. This ratio was determined in the present investigation for $c = 0$ and found to be a characteristic constant of the wind tunnel equal to 76.582 and independent of the wind velocity. The procedure followed to determine the ratio k_p/k_m is described below.

From Eq. (15) we have

$$\frac{k_p}{k_m} = \frac{y_p}{y_m} 10^{(u_m - U_{10})/5.75u*}. \quad (16)$$

It has already been established that in the prototype, for $c = 0$ and fully developed sea, the surface drift is given by

$$T = 0.033 U_{10}. \quad (17)$$

Substituting (17) into (16), yields

$$\frac{k_p}{k_m} = \frac{y_p}{y_m} 10^{[u_m - (T/0.033)]/5.75u*}. \quad (18)$$

For $c = 0$ and given air flow, the surface drift T and the corresponding wind velocity profile were determined in the model. Subsequently, the wind velocity u_m at height $y_m = 0.2$ ft as well as the shear velocity $u*$ were determined. Substituting these values and $y_p = 10$ m ≈ 32.8 ft into (18), the corresponding value of the ratio k_p/k_m was determined. This procedure was repeated for different air-flow rates and the corresponding values of the ratio k_p/k_m were determined. Finally, the average value of k_p/k_m was calculated and found to be equal to 76.582.

Considering also that for exact scaling it is required that the ratio $H_{1/3}/k$ be the same in the model and the prototype, it is concluded that

$$\frac{H_{p1/3}}{H_{m1/3}} = \frac{k_p}{k_m} = 76.582, \quad (19)$$

where $H_{m1/3}$ and $H_{p1/3}$ are the significant wave heights in the model and the prototype, respectively. Eq. (19) is the scaling law for the significant wave heights between the present model and the prototype. It is important to point out that (19) is the scaling law between the *present* model and the prototype and not an universal scaling law. In other words, the value of the ratio k_p/k_m is different for different current tank/wind tunnel configurations and should be determined following the procedure used in the present study.

At this point some comments are necessary on the meaning of the shear velocity $u*_p = u*_m$ and the surface roughness k_p determined in this study. The scaling law from model to prototype conditions, described earlier in this section, is based on the assumption that the dynamical process of wind-wave generation is the same in the model and the prototype. However, Wu (1972) has shown that the

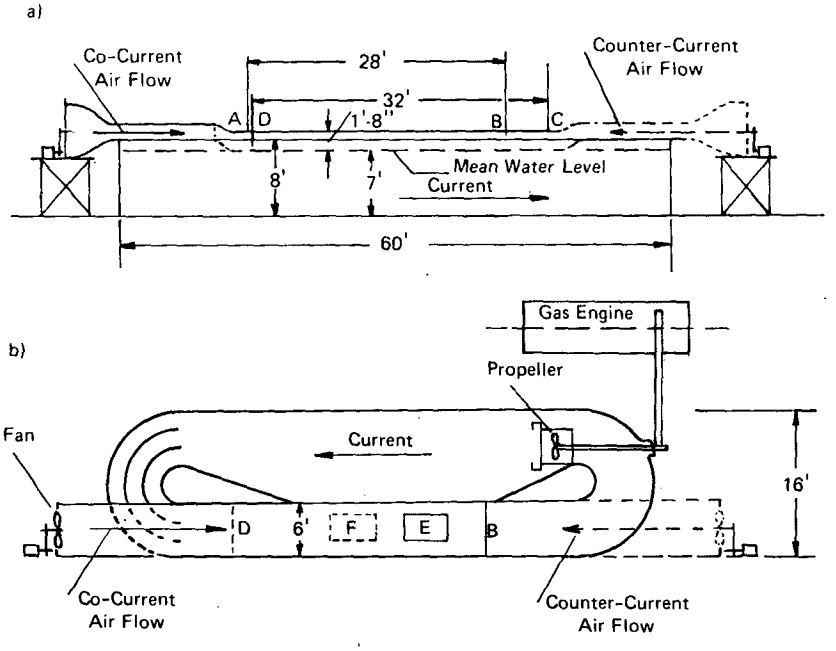

FIG. 3. Side view (a) and plan view (b) of current tank/wind tunnel.

air flow separates from dominant gravity waves in the model and from wavelets riding on top of dominant gravity waves in the prototype (ocean). In other words, the surface roughness k_m in the model is closely related to the significant wave height $H_{m1/3}$ of the dominant gravity waves where at high wind velocities $H_{m1/3}/k_m \approx 1$, while the surface roughness k_o in the ocean (the subscript o indicates oceanic conditions) is much smaller than the significant wave height $H_{p1/3}$ of the dominant gravity waves where at high wind velocities $H_{p1/3}/k_o \approx 100$ (Wu, 1972). Therefore, the shear velocity u_{*p} and the surface roughness k_p are related to the significant wave height $H_{p1/3}$ and not to the surface roughness k_o, i.e., $H_{p1/3}/k_p \approx 1$ since $H_{m1/3}/k_m \approx 1$ and $H_{p1/3}/k_p = H_{m1/3}/k_m$ under the present scaling law. Considering that $H_{p1/3}/H_{m1/3} = 76.582$, determined in the present study, it follows that

$$k_o = 0.01k_p = 0.766k_m. \tag{20}$$

It is evident from the above discussion that if u_{*o} is the shear velocity in the ocean related to the surface k_o, then the velocity U_{10} at height $y_p = 10$ m and the surface drift T_p, determined in the present study, satisfy the equation

$$\frac{U_{10} - T_p}{u_{*o}} = 5.75 \log\left(\frac{y_p}{k_o}\right) + 8.5. \tag{21}$$

Subtracting Eq. (21) from Eq. (14) and taking into account Eq. (20), it is determined that

$$u_{*o} = \frac{u_{*p}}{1 + 11.5\dfrac{u_{*p}}{U_{10} - T_p}}. \tag{22}$$

The above equation gives the shear velocity u_{*o} in oceanic conditions corresponding to the surface roughness k_o in terms of U_{10}, T_p, and $u_{*p} = u_{*m}$ determined in the present study.

The wind-stress coefficients in the model and the ocean, determined using Eq. (22), for $c = 0$, have been plotted versus the Froude number in Fig. 13. The very good agreement between the present results for $y = 10$ m and Wu (1969) data from 30 field observations attest to the validity of the scaling law employed in the present study.

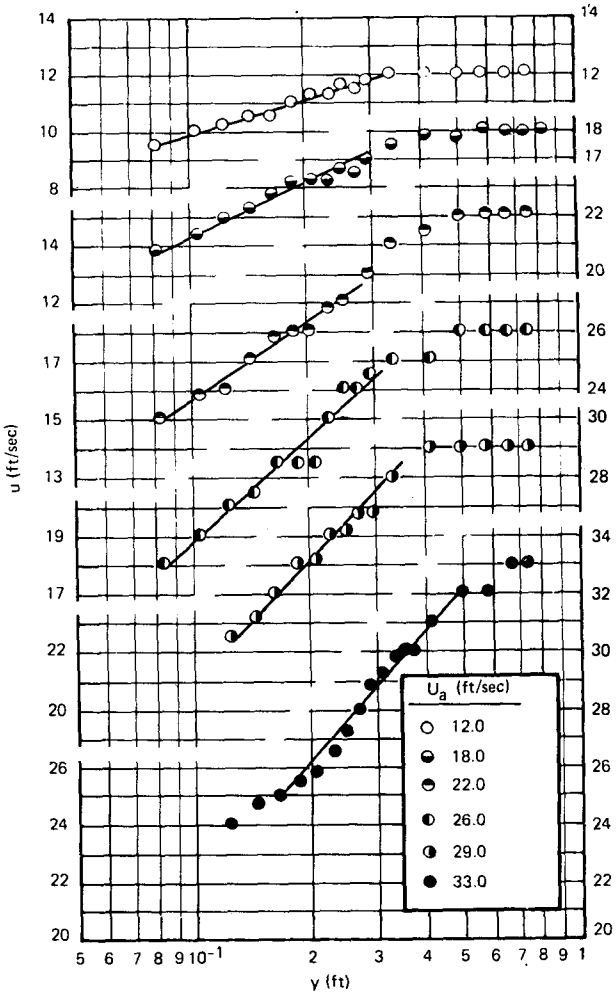

FIG. 4. The wind velocity u versus the distance y above the mean water level for different free-stream velocities and $c = 0$.

4. Experiments

The experiments were conducted at the closed-loop current tank of the Shell Pipeline Research and Development Laboratory, Shell Development Company, Fig. 3. The dimensions of the test section were 32 ft long, 6 ft wide, 7 ft deep. Currents were created by a variable-speed motor-driven propeller mounted at the return leg of the current tank. The

TABLE 3. Selected data of wind-induced drift for zero current.

U_a (ft s^{-1})	T (ft s^{-1})	u_* (ft s^{-1})	u_m ($y_m = 0.2$ ft) (ft s^{-1})	$k_m \times 10^2$ (ft)	$\frac{k_m u_*}{\nu_a}$ ($\nu_a = 1.6 \times 10^{-4}$) (ft^2 s^{-1})	U_{10} (ft s^{-1})	$\frac{k_p}{k_m}$
12.0	0.3948	0.7096	11.067	1.457	64.6	11.963	—
18.0	0.5922	1.1524	16.249	2.608	187.8	17.945	90.969
22.0	0.7238	1.4907	18.143	5.585	520.3	21.933	59.249
26.0	0.8554	2.0680	22.291	9.475	1224.6	25.921	81.202
29.0	0.9541	2.4287	25.252	10.949	1661.9	28.912	89.693
33.0	1.0857	2.8990	25.864	19.625	3555.8	32.900	62.051

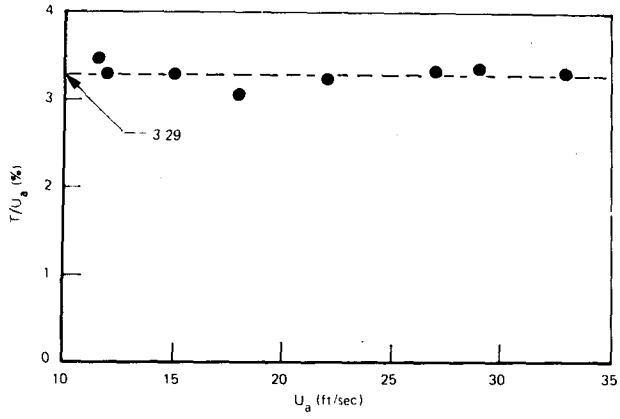

FIG. 5. The percent drift T/U_a versus the free-stream velocity U_a.

maximum obtainable current velocity was 2.5 ft s^{-1}. The top of the test section was covered to form the wind tunnel with a 20-inch deep air passage above the normal 7 ft water depth. A variable-speed motor-driven, 40 000 SCFM free discharge fan was used. A transition duct connected the 6 ft × 6 ft frame of the fan with the 20-inch by 6 ft cross section of the wind tunnel. The transition duct with the fan was mounted either at the upstream or the downstream end of the test section of the current tank so that cocurrent or countercurrent air flow was achieved, respectively. The minimum and maximum wind velocities obtainable with this configuration were 10 and 34 ft s^{-1}, respectively. Both the current tank and the wind tunnel were fitted with screens in order to provide uniform velocity profiles.

The closed-loop design of the current tank guaranteed that no subsurface backflow developed due to the wind- and wave-induced drift and that all waves, particularly the short, high-frequency waves, were not reflected back to the test section. Subsurface backflow and the reflection of waves are the major disadvantages of similar experiments in wave tanks or water basins. Furthermore, it was observed during the experiments that the maximum wavelength of the wind-generated waves was less than one-fourth of 1) the water depth, indicating

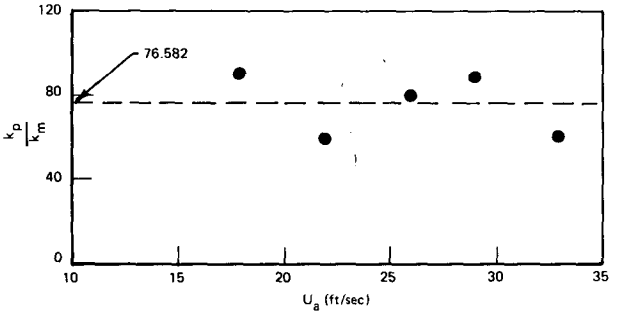

FIG. 6. The ratio of surface roughness k_p/k_m versus the free-stream velocity U_a.

TABLE 4. Selected data of wind-induced drift for cocurrent air flow, $c \neq 0$.

c (ft s^{-1})	U_a (ft s^{-1})	T (ft s^{-1})	u_* (ft s^{-1})	u_m (ft s^{-1})	U_{10} (ft s^{-1})	$\frac{T-c}{c}$	$\frac{U_{10}}{c}$
0.8922	10.75	1.1764	0.6400	9.457	10.674	0.318	11.963
	16.00	1.3333	1.1546	12.372	14.567	0.494	16.328
	20.00	1.4545	0.8797	16.127	17.799	0.630	19.950
	23.00	1.5306	1.4354	19.256	21.995	0.715	24.653
1.4630	22.50	2.0690	1.1796	20.041	22.284	0.414	15.230
1.5460	11.75	1.7640	0.6476	11.145	12.376	0.141	8.005
	16.00	1.8980	0.9889	14.865	16.745	0.228	10.831
	19.00	2.0400	1.1497	17.668	19.854	0.320	12.842
	23.75	2.2388	1.6534	21.298	24.442	0.448	15.809
	28.00	2.4000	1.8568	24.666	28.196	0.552	18.238
	33.00	2.5000	1.8847	28.201	31.785	0.617	20.559
2.0000	10.68	2.0830	0.5833	9.672	10.786	0.041	5.537
	17.00	2.3070	0.7770	15.366	16.843	0.153	8.421
	21.00	2.5000	1.0760	19.411	21.457	0.250	10.728
	25.00	2.6080	1.3630	22.434	25.025	0.304	12.512
	28.00	2.8570	1.6720	25.395	28.574	0.428	14.287
	33.00	3.0500	1.7340	29.244	32.541	0.525	16.270
2.4590	11.50	2.5000	0.5600	10.394	11.458	0.016	4.659
	18.50	2.7520	0.6900	17.339	18.651	0.119	7.584

that deep-water type waves were achieved, and 2) the wind-tunnel width, assuring no side-wall effect on the development of the wind profile. The flow in both the air and the water was turbulent. However, no measurements of the air turbulence were made because Reisbig *et al.* (1973) found that turbulence intensity has no effect on surface drift.

The surface drift was determined by measuring the time required by an oil slick to travel a distance of 6 ft. The oil slick was created by releasing 1–3 cm^3 of No. 6 oil at the centerline of the current tank. To establish a data point, three to five runs were carried out for a given set of conditions and used to give an average value. The timing of the oil slick was made through a 4 ft wide, 8 ft long plexiglass window fitted in the roof of the wind tunnel. The 6 ft long measuring station was placed 5 and 9 ft upstream of the exit and 17 ft downstream of the entrance of the wind tunnel for cocurrent and countercurrent air flow, respectively. This arrangement minimized wind-tunnel end-effects on the air-flow field and the surface drift. Furthermore, the small size of the oil slick with respect to the wavelength of waves with celerity larger than the surface drift guaranteed that the drift of the oil slick was the same with the surface drift of the uncontaminated water.

A Thermonetics type HWA-101, constant temperature hot-wire anemometer was used to determine the wind velocity profile. The support of the probe was mounted on a micrometer screw so that the hot-wire anemometer could be indexed vertically throughout the height of the wind tunnel. The traversing mechanism was located 15 and 25 ft from the entrance of the wind tunnel for cocurrent and countercurrent air flow, respectively.

The following procedure was used in the experiments. The motor of the current tank was started and the water flow was allowed to reach steady state. The current velocity c (surface drift for zero wind velocity) was determined by the method described earlier. The motor of the fan was started and the air flow was adjusted so that the maximum wind velocity reached a desired value. Enough time was allowed so that the wind-generated waves and the total surface drift, i.e., the combined current, wind- and wind-generated wave-induced drift, reached a steady state. Then the total surface drift T was determined by the method described earlier. The wind velocity profile $u_m(y)$, where y is the height from the mean water level, was determined by the vertical traverse of the hot-wire anemometer. This concluded the run for this wind speed. The same procedure was repeated for different wind velocities. This concluded the run for this current velocity.

5. Experimental results

a. Zero current velocity, $c = 0$

The wind velocity profiles, measured at different free-stream velocities, are plotted in Fig. 4. The free-stream velocity U_a was determined from the middle flat part of the wind velocity profile. The straight-line portion of each velocity profile indicates that the wind velocity profile is logarithmic over this portion, in agreement with the experimental findings of Wu (1968) and Shemdin (1972). The slope of these straight lines is proportional to the shear velocity $u*$. Wu (1968) established experimentally that the constant of proportionality is the universal constant (5.75) in the Kármán-Prandtl velocity distribution [Eqs. (13) or (14)]. The resulting shear velocities are given in Table 3.

The surface drift T was determined for different free-stream velocities. In Fig. 5, the percent drift, based on the free-stream velocity, is plotted versus the free-stream velocity. It is seen that the percent drift remains fairly constant for different free-stream velocities. The average percent drift is equal to 3.29% with a standard deviation of 3.57% or 0.117% drift units. The average percent drift was used to calculate the surface drifts given in Table 3.

The surface roughness was calculated from Eq. (13) and can be written as

$$k_m = y_m 10^{(8.5u* + T - u_m)/5.75u*}. \tag{23}$$

TABLE 5. Selected data of wind-induced drift for countercurrent air flow, $c \neq 0$.

c (ft s^{-1})	$-U_a$ (ft s^{-1})	T (ft s^{-1})	$u*$ (ft s^{-1})	$-u_m$ (ft s^{-1})	$-U_{10}$ (ft s^{-1})	$-\frac{T-c}{c}$	$-\frac{U_{10}}{c}$
0.6081	28.00	−0.3125	1.8750	23.468	27.033	1.513	44.455
0.6198	12.50	0.3526	0.5939	10.587	11.716	0.431	18.902
0.6269	16.50	~0.0	0.8281	16.561	18.136	~1.0	28.930
	22.00	~0.0	1.2013	18.330	20.615	~1.0	32.884
	26.00	−0.1797	1.7168	21.905	25.170	1.286	40.149
	32.00	−0.3794	2.1850	26.505	30.660	1.605	48.907
0.7450	11.25	0.5070	0.4656	9.916	10.801	0.319	14.497
	18.75	~0.0	0.9138	16.713	18.451	~1.0	24.766
	24.00	~0.0	1.2600	20.159	22.555	~1.0	30.276
	27.00	−0.1840	1.8737	23.035	26.598	1.246	35.702
0.7595	32.00	−0.2624	2.0687	27.259	31.193	1.345	41.070
0.9418	18.00	0.5050	0.6422	16.546	17.767	0.464	18.865
	22.00	0.4149	1.4991	18.380	21.231	0.559	22.543
	28.00	0.2052	1.5502	24.866	27.814	0.782	29.533
	31.00	~0.0	2.0850	27.048	31.030	~1.0	32.930
1.5375	11.50	1.3760	0.5594	10.213	11.276	0.105	7.334
	18.00	1.2370	0.8255	16.605	18.174	0.195	11.821
	22.00	1.0877	1.7313	19.353	22.645	0.292	14.728
	28.00	1.0000	1.8288	23.313	26.791	0.349	17.424
	33.00	0.7983	2.0430	26.744	30.629	0.481	19.921
1.9675	11.00	1.8730	0.5836	9.412	10.521	0.048	5.347
	16.50	1.6783	1.0050	14.112	16.024	0.147	8.144
	22.00	1.5650	1.6285	18.129	21.226	0.204	10.788
	27.00	1.4280	1.9829	23.000	26.770	0.272	13.606
2.1810	11.00	2.0935	0.5781	9.217	10.316	0.040	4.729
	18.25	1.8750	0.8826	15.733	17.412	0.140	7.983
	23.00	1.6660	1.5020	18.303	21.160	0.236	9.701
	27.25	1.5380	1.7880	23.929	27.329	0.294	12.530
	32.50	1.4064	1.8340	28.728	32.216	0.355	14.771

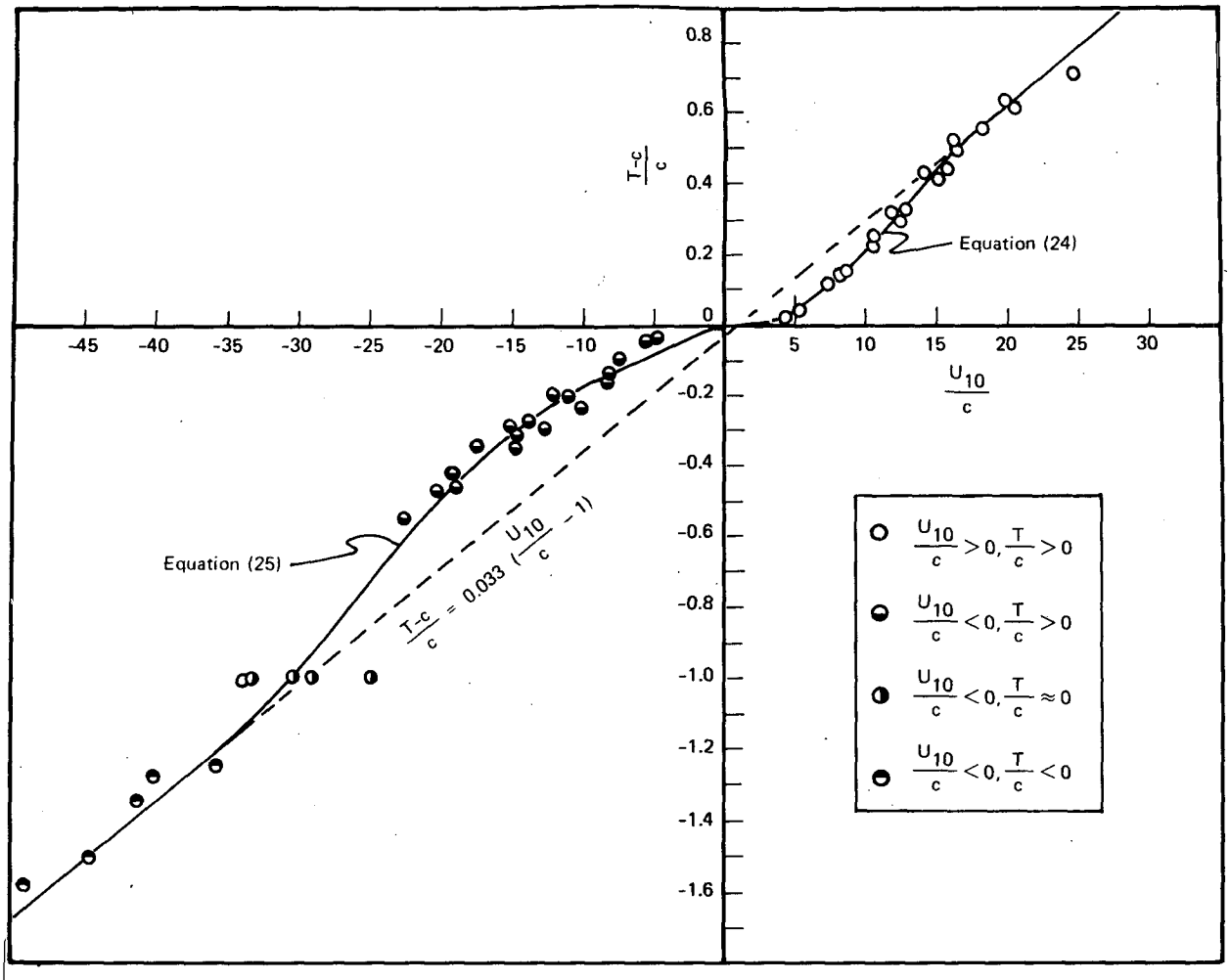

FIG. 7. The surface drift ratio $(T - c)/c$ versus the ratio U_{10}/c.

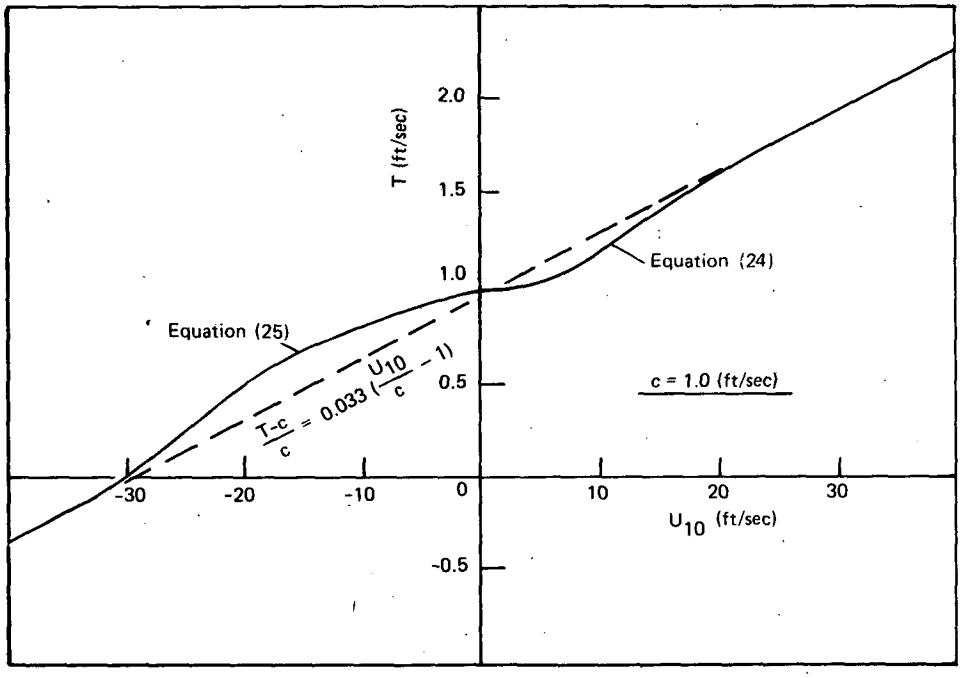

FIG. 8. The combined drift T, calculated from Eqs. (24)–(25) for $c = 1$ ft s^{-1}, versus the wind velocity U_{10}.

In Eq. (23), the wind velocity u_m at $y_m = 0.2$ ft was calculated from the linear fit of the logarithmic portion of the wind velocities profiles (see Fig. 4). The resulting surface roughnesses and wind velocities are given in Table 3. The corresponding wind velocities of the prototype, U_{10}, were calculated from Eq. (17) and are also given in Table 3.

The values of the nondimensional group $u_* k/\nu_a$ were also calculated and are given in Table 3. It is seen that for $U_a = 12$ ft s^{-1}, $u_* k/\nu_a = 64$. Since for exact scaling it is required that $u_* k/\nu_a > 70$, this case was excluded from the calculation of the ratio k_p/k_m. The ratios k_p/k_m of surface roughnesses, were finally calculated from Eq. (18). They are given in Table 3 and are also plotted in Fig. 6 as a function of the free-stream velocity. It is seen that the ratio k_p/k_m remains fairly constant for different free-stream velocities. The average value of k_p/k_m is equal to 76.582 with a standard deviation of 19.7% or 15 units. This value of k_p/k_m was used for the scaling of the experimental results from the model to the prototype for $c \neq 0$:

b. Cocurrent air flow, $c \neq 0$

The surface drift T, the shear velocity u_*, and the wind velocity u_m at $y_m = 0.2$ ft were determined at different freestream velocities for nonzero current c. The corresponding wind velocity profiles were found to follow the logarithmic law near the water surface as in the case $c = 0$. The quantities c, T, u_* and u_m were determined in exactly the same way as for $c = 0$. The corresponding wind velocities of the prototype, U_{10}, were calculated from Eq. (15), where $y_p = 10$ m ≈ 32.8 ft and $k_p/k_m = 76.582$. All the above data as well as the corresponding values of the ratios $(T - c)/c$ and U_{10}/c are compiled in Table 4.

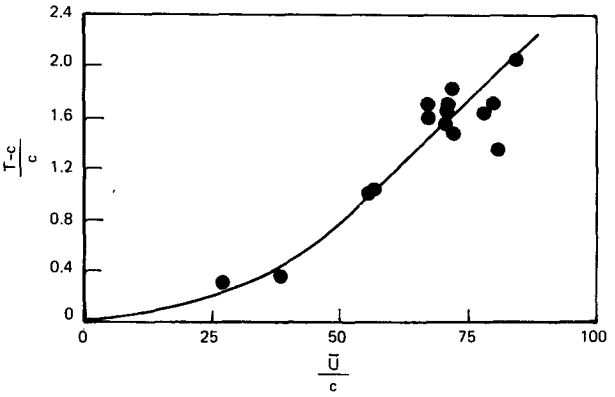

FIG. 9. The surface drift ratio $(T - c)/c$ versus the ratio $\bar{U}/c$ from Schwartzberg (1970).

c. Countercurrent air flow, $c \neq 0$

The surface drift T, the shear velocity u_*, the wind velocity u_m at $y_m = 0.2$ ft, and the wind velocity of the prototype, U_{10}, were determined at different free-stream velocities for nonzero current c. Again the corresponding velocity profiles were found to follow the logarithmic law near the water surface. All the above data as well as the corresponding values of the ratios $(T - c)/c$ and U_{10}/c are compiled in Table 5.

6. Discussion

a. Combined drift for cocurrent and countercurrent air flow

The combined drift data for cocurrent and countercurrent air flow, given in Tables 4 and 5, are plotted in Fig. 7. The proper choice of the nondimensional groups $(T - c)/c$ and U_{10}/c for the description of the combined current, wind- and

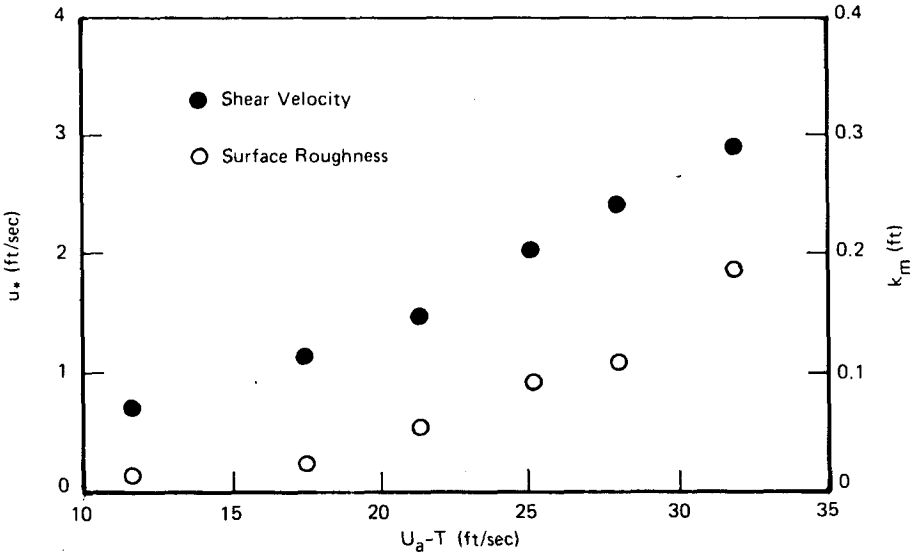

FIG. 10. The shear velocity u_* and the surface roughness k_m versus the relative free-stream velocity $U_a - T$.

wind-generated wave-induced drift, as discussed in Section 2, is reflected by the small scatter of the data points. Consequently, the total surface drift can be expressed by Eq. (10), i.e., $(T - c)/c = f(U_{10}/c)$. Furthermore, it is seen in Fig. 7 that 1) $\lim f(U_{10}/c) \to 0$ as $|(U_{10}/c)| \to 1$ and 2) $\lim(U_{10}/c) \to 0.033[(U_{10}/c) - 1]$ as $|(U_{10}/c)| \to |(U_{10}/c_{cr}|$, as was predicted in Section 2 [see Eqs. (11) and (12), respectively].

The combined-drift data are correlated by the following expressions:

1) COCURRENT AIR FLOW:

$$\frac{U_{10}}{c} > 0, \qquad \frac{U_{10}}{c} < 20 = \left(\frac{U_{10}}{c}\right)_{cr}.$$

$$\frac{T-c}{c} = -0.1050527089 \times 10^{-3} + 0.1500198899 \times 10^{-2}\left(\frac{U_{10}}{c}\right) - 0.2293448363 \times 10^{-2}\left(\frac{U_{10}}{c}\right)^2 + 0.1095792709 \times 10^{-2}\left(\frac{U_{10}}{c}\right)^3 - 0.1016695711 \times 10^{-3}\left(\frac{U_{10}}{c}\right)^4 + 0.4264489226 \times 10^{-5}\left(\frac{U_{10}}{c}\right)^5 - 0.8603259619 \times 10^{-7}\left(\frac{U_{10}}{c}\right)^6 + 0.6782270924 \times 10^{-9}\left(\frac{U_{10}}{c}\right)^7, \quad (24)$$

with standard deviation 0.0169191.

2) COUNTERCURRENT AIR FLOW:

$$\frac{U_{10}}{c} < 0, \qquad \frac{U_{10}}{c} > -35 = \left(\frac{U_{10}}{c}\right)_{cr}$$

$$\frac{T-c}{c} = -0.2701343473 \times 10^{-2} + 0.7098815489 \times 10^{-2}\left(\frac{U_{10}}{c}\right) - 0.3906915993 \times 10^{-2}\left(\frac{U_{10}}{c}\right)^2 - 0.5514315187 \times 10^{-3}\left(\frac{U_{10}}{c}\right)^3 - 0.3788438367 \times 10^{-4}\left(\frac{U_{10}}{c}\right)^4 - 0.1221455396 \times 10^{-5}\left(\frac{U_{10}}{c}\right)^5 - 0.1845871780 \times 10^{-7}\left(\frac{U_{10}}{c}\right)^6 - 0.1062438968 \times 10^{-9}\left(\frac{U_{10}}{c}\right)^7, \quad (25)$$

with standard deviation 0.0290561.

3) (i) COCURRENT AIR FLOW: $\frac{U_{10}}{c} > 20$

(ii) COUNTERCURRENT AIR FLOW:

$$\frac{U_{10}}{c} < -35$$

(iii) $c = 0$

$$\frac{T-c}{c} = 0.033\left(\frac{U_{10}}{c} - 1\right). \quad (26)$$

As it is shown in cases 1) and 2), the critical values of the ratio U_{10}/c are 20 and -35 for cocurrent and countercurrent air flow, respectively.

In Fig. 8, the combined drift T, calculated from (24)–(26) for $c = 1$ ft s^{-1}, is plotted versus the wind velocity U_{10}. The surface drift calculated from (8), where the effect of the wave-induced motion is not taken into account, is also plotted in Fig. 8. It is seen that the waves cause a net decrease or increase of the combined drift for cocurrent or countercurrent air flow, respectively. This effect disappears for $|(U_{10}/c)| > |(U_{10}/c)_{cr}|$. This is not surprising since the effect of waves on the surface drift has been taken implicitly into account in Eq. (8) when $|(U_{10}/c)| > |(U_{10}/c)_{cr}|$. It should be mentioned that Reisbig *et al.* (1973) also determined experimentally that, for waves and winds traveling in the same direction, the waves cause a net decrease of the combined drift for wind speeds >2.6 ft s^{-1}.

The only available experimental data on combined drift for nonzero current are the one by Schwartzberg (1970). Unfortunately, his results cannot be compared with the present results because he only

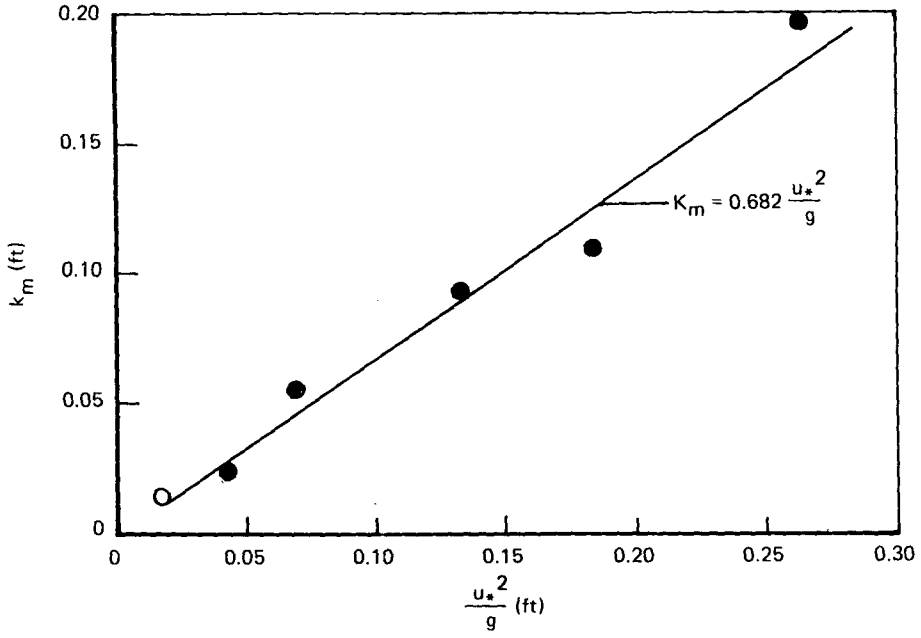

FIG. 11. The surface roughness versus the ratio u_*^2/g.

measured the mean wind velocity $\bar{U}$ through his wind tunnel. However, his data are plotted in Fig. 9 in terms of the ratios $(T - c)/c$ and $\bar{U}/c$. It is seen that, in spite the fact that $\bar{U}$ has been used in place of U_{10}, the data points can be correlated by a single curve. This is another verification of the proper selection of the nondimensional groups $(T - c)/c$ and U_{10}/c for the description of the combined drift.

b. Surface roughness, shear velocity and wind stress coefficient for $c = 0$

In Fig. 10, the shear velocity u_* and the surface roughness k_m given in Table 3 are plotted as a function of the free-stream velocity relative to the moving water surface, $U_c = U_a - T$. It is seen that for completely rough flow, i.e., excluding the case $U_a = 12$ ft s^{-1}, $k_m U_*/\nu_a < 70$, both u_* and k_m increase approximately linearly with U_c. Wu (1968) also found the same dependence of u_* and k_m on U_c for completely rough flow (after wave breaking).

Charnock (1955) suggested on physical arguments that

$$\frac{k}{u_*^2/g} = \text{constant} \qquad (27)$$

for completely rough flow due to gravity waves. In the present experiments gravity waves were generated and the flow was aerodynamically rough, except for $U_a = 12$ ft s^{-1}. Thus, Charnock's argument can be tested, as shown in Fig. 11, where the

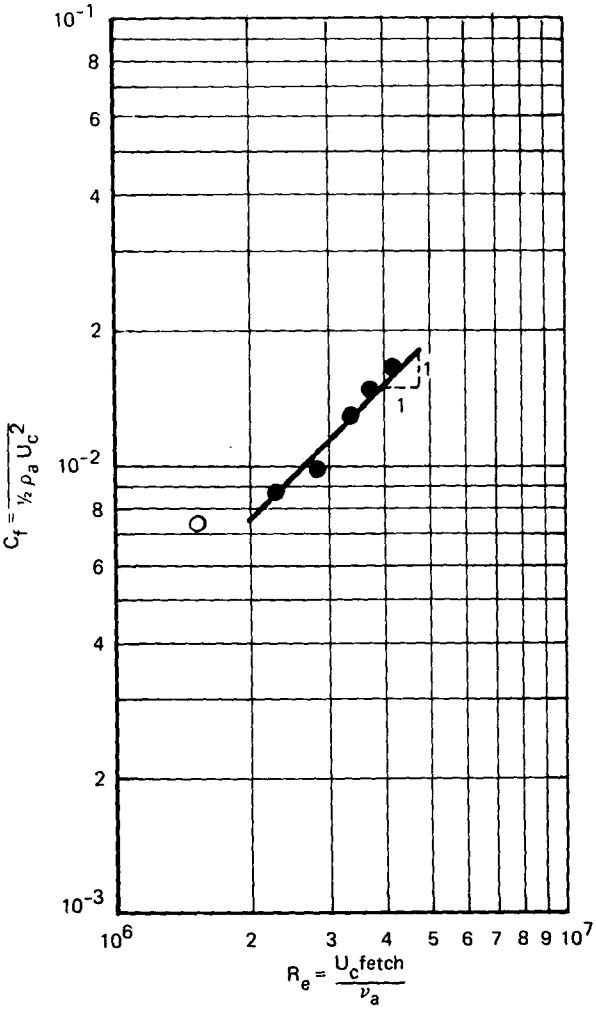

FIG. 12. The wind stress coefficient versus the Reynolds number.

surface roughness k_m is plotted as a function of the ratio u_*^2/g. It is seen that the data can be fitted with a straight line. The proportionality constant in (27) was determined to be 0.682. In his laboratory studies Wu (1968) determined the proportionality constant to be 0.337 then he adjusted it (1969) to 0.468 by fitting wind-stress data from 42 independent investigations—12 laboratory studies and 30 field observations—and finally he determined (Wu, 1970) that the constant is 0.814 by fitting only the 30 oceanic data. It appears that the value of the proportionality constant in Charnock's expression determined in the laboratory depends on the experimental set-up and that the value 0.814 determined from oceanic data only is the correct one.

In Fig. 12, the wind-stress coefficient C_f is plotted versus the Reynolds number $\mathrm{Re} = (U_c) \times (\text{fetch})/\nu_a$, where the fetch is the distance between the entrance of the wind tunnel and the measuring station. It is seen that for completely rough flow (solid circles) the wind-stress coefficient changes almost linearly with U_c, in agreement with the experimental findings of Wu (1968).

In Fig. 13, the wind-stress coefficients in the model, $C_y = (u_{*m}/u_m)^2$, and the prototype (oceanic conditions), $C_y = (u_{*o}/U_{10})^2$, are plotted versus the Froude number, $\mathrm{F} = U_y/(gy)^{1/2}$, where $U_y = U_{10}$, $y = 10$ m, and $U_y = u_m$, $y = 0.2$ ft, for the prototype and the model, respectively. In the same figure the curves obtained from

$$\frac{1}{C_y^{1/2}} = \frac{1}{k} \ln\left(\frac{30}{aC_y\mathrm{F}^2}\right), \qquad (28)$$

where $k = 0.4$ is the Kármán constant, are also plotted for the previously mentioned different values of Charnock's proportionality constant a. Eq. (28) was proposed and verified by Wu (1969) for the Froude number scaling of wind-stress coefficients. As pointed out earlier, the very good agreement of the present results for $y = 10$ m with the oceanic data attest to the validity of the scaling law employed in the present study.

7. Summary and conclusions

The surface drift on open water due to the combined action of currents, winds and wind-generated

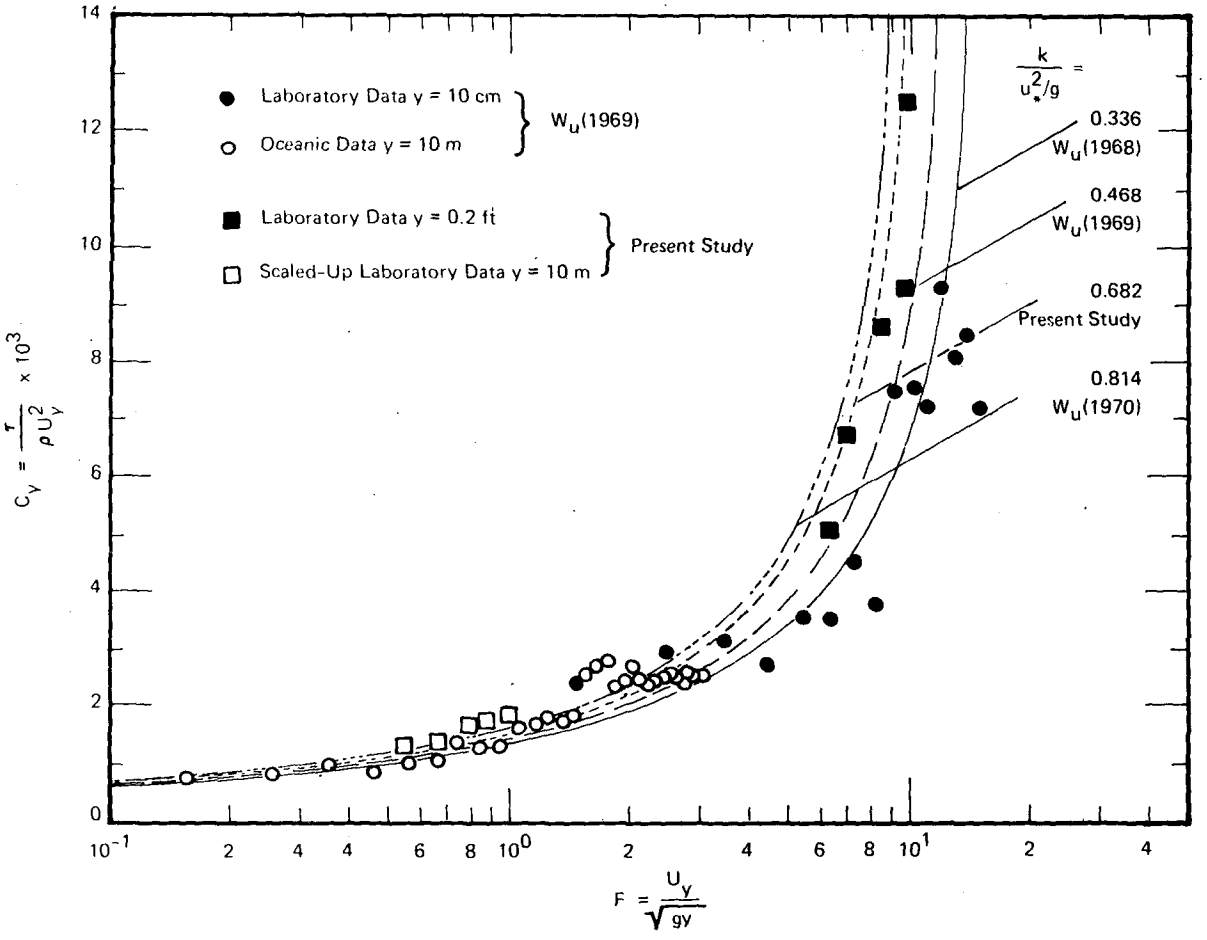

FIG. 13. Froude scaling of wind-stress coefficient.

waves has been studied both theoretically and experimentally for cocurrent and countercurrent air flow.

It has been shown theoretically that the nondimensional groups necessary for the modeling of surface drift are $(T - c)/c$ and U_{10}/c, where U_{10}, T and c are the wind, water surface and current velocities, respectively, the wind being measured at the uniquely adopted height of 10 m. Surface drift experiments, carried out in a current tank/wind tunnel, have verified the theoretically predicted dependence on the above groups and led to the derivation of relationships for the calculation of the total surface drift. The present results show that wind-generated waves generally cause a net decrease or increase of the surface drift for cocurrent or countercurrent air flow, respectively.

The surface drifts, calculated from the above relationships, are in excellent agreement with available field and laboratory data.

Laws have been formulated for the scaling of current tank/wind tunnel data for wind velocities and significant wave heights to prototype (atmospheric boundary layer) conditions.

The present experimental results confirm that the wind velocity distribution follows the logarithmic law near the water surface. For zero current and completely rough water surface, the shear velocity, the surface roughness and the wind stress coefficient are found to increase linearly with the free-stream wind velocity relative to the moving water surface. Furthermore, the present results support Charnock's expression relating the surface roughness and shear velocity for completely rough flow due to gravity waves and Wu's Froude number scaling of wind-stress coefficients.

REFERENCES

Alofs, D. J., and R. L. Reisbig, 1972: An experimental evaluation of oil slick movement caused by waves. *J. Phys. Oceanogr.*, **2,** 439–443.

Bye, J. A. T., 1967: The wave-drift current. *J. Mar. Res.*, **25,** 95–102.

Charnock, H., 1955: Wind stress on a water surface. *Quart. J. Roy. Meteor. Soc.*, **81,** 639–640.

Fitzgerald, L. M., 1964: The effect of wave-damping on the surface velocity. *Aust. J. Phys.*, **17,** 184–188.

Hughes, P., 1956: A determination of the relation between wind and sea-surface drift. *Quart. J. Roy. Meteor. Soc.*, **82,** 492–502.

Kenyon, K. E., 1969: Stokes drift for random gravity waves. *J. Geophys. Res.*, **74,** 6991–6994.

Keulegan, G. H., 1951: Wind tides in small closed channels. *J. Res. Nat. Bur. Stnd.*, **46,** 358–381.

Kraus, E. B., 1977: Ocean surface drift velocities. *J. Phys. Oceanogr.*, **7,** 606–609.

Madsen, O. S., 1977: Realistic model of the wind-induced Ekman boundary layer. *J. Phys. Oceanogr.*, **7,** 248–255.

Monin, A. S., 1969: Fundamental consequences of the interaction between atmosphere and ocean. *J. Atmos. Ocean. Phys.*, **5,** 635–640.

Pierson, W. J., G. Newmann and R. W. James, 1955: H. O. Publ. No. 603, U.S. Navy Hydrographic Office, Washington DC.

Plate, E., 1971: Aerodynamic characteristics of atmospheric boundary layers, 1st ed. USAEC Tech. Inform. Center, Oak Ridge, Tenn.

——, and M. Trawle, 1970: A note on the celerity of wind waves on a water current. *J. Geophys. Res.*, **75,** 3537–3544.

Reisbig, R. L., D. J. Alofs, R. C. Shah and S. K. Banerjee, 1973: Measurement of oil spill drift caused by the coupled parallel effects of winds and waves. *Mém. Soc. Roy. Sci. Liège*, **6,** 67–77.

Ruggles, K. W., 1969: Observations of the wind field in the first ten meters of the atmosphere above the ocean. Dept. of Meteor., MIT, Rep. 69–1.

Schwartzberg, H. G., 1970: Spreading and movement of oil spills. Dept. of Chem. Eng., New York University, Publ. PB192852.

Schlichting, H., 1968: *Boundary Layer Theory*, 6th ed. McGraw Hill.

Shemdin, O. H., 1972: Wind-generated current and phase speed of wind waves. *J. Phys. Oceanogr.*, **2,** 411–419.

Smith, C. L., 1974: Determination of the leeway of slicks. U.S. Coast Guard Rep. No. CG-D-60-75, Virginia Institute of Marine Science.

Smith, J. E., 1968: Torrey Canyon pollution and marine life. Cambridge University Press.

Tomczak, G., 1964: Investigations with drift cards to determine the influence of the wind on surface currents. *Stud. Oceanogr.*, University of Washington, 129–139.

Van Dorn, W. G., 1953: Wind stress of an artificial pond. *J. Mar. Res.*, **12,** 249–276.

Wright, J. W., and W. C. Keller, 1971: Doppler spectra in microwave scattering wind waves. *Phys. Fluids*, **14,** 466–474.

Wu, J., 1968: Laboratory studies of wind-wave interactions. *J. Fluid Mech.*, **34,** 91–111.

——, 1969: Froude number scaling of wind-stress coefficients. *J. Atmos. Sci.*, **26,** 408–413.

——, 1970: Wind-wave interaction. *Phys. Fluids*, **13,** 1926–1930.

——, 1972: Physical and dynamical scales for generation of wind waves. *J. Water., Harbors, Coastal Engr. Div.*, **98,** 163–175.

——, 1975: Sea surface drift currents. *Proc. Offshore Technology Conf.*, Houston, Paper No. OTC 2294.